α particles and the "pasta" phase in nuclear matter

S. S. Avancini,[1] C. C. Barros Jr.,[1] D. P. Menezes,[1] and C. Providência[2]
[1]*Departamento de Física, CFM, Universidade Federal de Santa Catarina Florianópolis SC, CP 476, CEP 88.040 900, Brazil*
[2]*Centro de Física Computacional, Department of Physics, University of Coimbra, P 3004 516, Coimbra, Portugal*
(Received 4 March 2010; revised manuscript received 24 June 2010; published 20 August 2010)

The effects of the α particles in nuclear matter at low densities are investigated within three different parametrizations of relativistic models at finite temperature. Both homogeneous and inhomogeneous matter (pasta phase) are described for neutral nuclear matter with fixed proton fractions and stellar matter subject to β equilibrium and trapped neutrinos. In homogeneous matter, α particles are present only at densities below 0.02 fm^{-3} and their presence decreases with increase of the temperature and, for a fixed temperature, the α particle fraction decreases for smaller proton fractions. A repulsive interaction is important to mimic the dissolution of the clusters in homogeneous matter. The effect of the α particles on the pasta structure is very small except close to the critical temperatures and/or proton fractions, when it may still predict a pasta phase while no pasta phase would occur in the absence of light clusters. It is shown that for densities above 0.01 fm^3 the α-particle fraction in the pasta phase is much larger than that in homogeneous matter.

DOI: 10.1103/PhysRevC.82.025808 PACS number(s): 21.65.−f, 24.10.Jv, 26.60.−c, 95.30.Tg

I. INTRODUCTION

The pasta phase is a frustrated system [1–5] present at densities of the order of 0.006–0.1 fm^{-3} [6] in neutral nuclear matter and 0.029–0.065 fm^{-3} [7,8] in β-equilibrium stellar matter, where a competition between the strong and the electromagnetic interactions takes place.

The basic shapes of these complex structures were named [1] after well-known types of cheese and pasta: droplets = meat balls (bubbles = Swiss cheese), rods = spaghetti (tubes = penne), and slabs = lasagna, for three, two, and one dimensions respectively. The pasta phase is the ground state configuration if its free energy per particle is lower than that corresponding to the homogeneous phase at the same density.

A complete equation of state capable of describing matter ranging from very low densities to a few times saturation density and from zero temperature to around 100 MeV is a necessary step toward the understanding of the stellar core collapse, supernova explosion, and protoneutron star evolution. The constitution of the pulsar crust plays a definite role in the emission of neutrino and gravitational waves. In the inner crust of neutron stars (zero temperature, very low proton fraction, matter in β equilibrium), the pasta phase is expected to be present and to coexist with a neutron gas. In a supernova (finite temperature, proton fraction around 0.3) the pasta phase is structured in such a way that there is no neutron gas or it is very low in density [9].

In previous works [6,8] we have studied the existence of the pasta phase at zero and finite temperature within different parametrizations of the relativistic nonlinear Walecka model (NLWM) [10], namely, NL3 [11], TM1 [12], and GM3 [13], and the onset of the pasta phase with different parametrizations of the density-dependent hadronic model, namely, TW [14], density dependent hadronic model with δ meson (DDHδ) [15], and GDFM [16,17], respectively. In these works two different methods were used: coexisting phases (CPs) at both zero and finite temperature and the Thomas-Fermi (TF) approximation at zero temperature only. It was found that matter in β equilibrium presents a small (at zero or small temperatures) or nonexistent pasta structure (at finite temperature above $\sim$4 MeV) [6]. In fact, even for Skyrme forces it was shown that, depending on the model, above 2–4 MeV there is no pasta phase for β equilibrium matter [18]. If β equilibrium is imposed, the pasta phase could not be found in a CP calculation for the same surface energy parametrization used for fixed proton fractions. This indicates the necessity to use a good parametrization for the surface energy that is temperature, proton fraction, and geometry dependent, as also stressed in [16,17]. The specific problem of an appropriate parametrization for the surface energy is tackled in the present work.

In the above calculations we have assumed predefined shapes for the pasta clusters and considered that the ground state configuration is the one that minimizes the free energy. In [19] the authors could show by using *ab initio* numerical simulations that in fact pasta phases can be formed in collapsing supernovas. By compressing a bcc lattice of spherical nuclei it was shown that an ordered structure of rod-like nuclei could be formed.

The importance of the α particles has been pointed out in the recent literature [20–24]. It is the most strongly bound system among all light systems and it certainly plays a role in nuclear matter. Lattimer and Swesty worked out the equation of state (EOS) in the compressible extended liquid drop model based on a nonrelativistic framework [20] appropriate for supernova simulations, for a wide range of densities, proton fractions and temperatures, including the contribution of α-particle clusters. An excluded volume prescription is used to model the dissolution of α particles at high densities. The same is done by Shen *et al.* in [21,25] where nonuniform matter composed of protons, neutrons, α particles, and single species of heavy nuclei is described with the Thomas-Fermi approximation and the TM1 parametrization of the nonlinear Walecka model. At low densities, these particles are approximated by classical gases. In [26] nuclear statistical equilibrium equations are calculated and the α particles are also taken into account.

In [22] an effective four-body equation that includes self-energy corrections and Pauli blocking is used in a consistent way. The influence of cluster formation on the nuclear matter EOS is calculated and the occurrence of instabilities is investigated in [27]. In [23] the virial equation of state of low-density nuclear matter composed of neutrons, protons, and α particles is presented, and it is shown that the predicted α-particle concentrations differ from the predictions of the EOSs proposed in [20] and [25]. The inclusion of small clusters in the EOS is reconsidered in [24], where the most important thermodynamical quantities are calculated with light clusters up to the α particle with a density-dependent relativistic model. The conditions for the liquid-gas phase transition are obtained, and it is seen how the binodal section is affected by the inclusion of these clusters. Moreover, an EOS is obtained starting at low densities with clusterized matter up to high density cluster-free homogeneous matter.

In the present paper we investigate the influence of the α particles both on the homogeneous matter and on the onset, size of the clusters, and structure of the pasta phase within the relativistic mean field approximation. As all results so far show model dependence, three different parametrizations are employed. We have chosen the NL3 [11] and GM1 [13] parametrizations of the NLWM and the TW parametrization of the density-dependent hadronic model [14]. The calculations are carried out for fixed proton fractions and also for matter in β equilibrium with trapped neutrinos. Although in previous works it was found that matter in β equilibrium presents a small (at zero temperature) or nonexistent pasta structure (at finite temperature) that is very sensitive to the surface energy [6,8], once trapped neutrinos are present, the picture changes considerably because of the large fraction of protons. According to studies on binodals and spinodals underlying the conditions for phase coexistence and phase transitions [18,28], nonhomogeneous matter with trapped neutrinos is expected to be found until temperatures around $T = 12$ MeV, depending on the model considered. For this reason, we investigate this possibility next.

The paper is organized as follows. In Sec. II we briefly review the formalism underlying the homogeneous neutral npe matter with the inclusion of the α particles. In Sec. III the pasta phase is built with the help of the coexisting phase method and the prescription for the introduction of the α's is given. A complete study for the parametrization of the surface energy based on the Thomas-Fermi calculation is performed and presented in Sec. IV. In Sec. V our results are displayed and commented on, and in Appendix our conclusions are drawn.

II. THE FORMALISM

We consider a system of protons and neutrons with mass M interacting with and through an isoscalar-scalar field ϕ with mass m_s, an isoscalar-vector field V^μ with mass m_v, and an isovector-vector field $\mathbf{b}^\mu$ with mass m_ρ. We also include α particles as bosons with mass M_α and a system of electrons with mass m_e. We do not consider models with δ mesons, but their introduction is straightforward. The Lagrangian density reads

$$\mathcal{L} = \sum_{i=p,n} \mathcal{L}_i + \mathcal{L}_e + \mathcal{L}_\sigma + \mathcal{L}_\omega + \mathcal{L}_\rho + \mathcal{L}_\alpha, \tag{1}$$

where the nucleon Lagrangian reads

$$\mathcal{L}_i = \bar{\psi}_i[\gamma_\mu i D^\mu - M^*]\psi_i, \tag{2}$$

with

$$i D^\mu = i\partial^\mu - \Gamma_v V^\mu - \frac{\Gamma_\rho}{2}\boldsymbol{\tau}\cdot\mathbf{b}^\mu - e\frac{1+\tau_3}{2}A^\mu, \tag{3}$$

$$M^* = M - \Gamma_s\phi. \tag{4}$$

The α particles are described as in [24] by

$$\mathcal{L}_\alpha = \tfrac{1}{2}\left(i D^\mu_\alpha \phi_\alpha\right)^*(i D_{\mu\alpha}\phi_\alpha) - \tfrac{1}{2}\phi^*_\alpha M^2_\alpha \phi_\alpha, \tag{5}$$

with

$$i D^\mu = i\partial^\mu - \Gamma_\alpha V^\mu, \tag{6}$$

where

$$M_\alpha = 4M - B_\alpha, \quad B_\alpha = 28.3\ \text{MeV}, \tag{7}$$

and Γ_α is included for mimicking the excluded volume effect and consequent α-particle dissolution at high densities. In [24] a more complete effective interaction for the α particles is considered, including the σ meson–α particle interaction and the Pauli shifts for the binding energy. In our approach we calculate a lower bound for the α particles present in the medium. As a reference we also consider the opposite limit and take the α particles as a gas of free particles. In most of our calculations Γ_α is set either to zero or to $\Gamma_\alpha = 4\Gamma_v$. We have also made tests using a lower value for this interaction ($2\Gamma_v$) and the results are noted when appropriate.

The electron Lagrangian density is given by

$$\mathcal{L}_e = \bar{\psi}_e[\gamma_\mu(i\partial^\mu + eA^\mu) - m_e]\psi_e, \tag{8}$$

and the meson Lagrangian densities are

$$\mathcal{L}_\sigma = +\frac{1}{2}\left(\partial_\mu\phi\partial^\mu\phi - m_s^2\phi^2 - \frac{1}{3}\kappa\phi^3 - \frac{1}{12}\lambda\phi^4\right),$$

$$\mathcal{L}_\omega = \frac{1}{2}\left(-\frac{1}{2}\Omega_{\mu\nu}\Omega^{\mu\nu} + m_v^2 V_\mu V^\mu + \frac{1}{12}\xi g_v^4 (V_\mu V^\mu)^2\right),$$

$$\mathcal{L}_\rho = \frac{1}{2}\left(-\frac{1}{2}\mathbf{B}_{\mu\nu}\cdot\mathbf{B}^{\mu\nu} + m_\rho^2\mathbf{b}_\mu\cdot\mathbf{b}^\mu\right),$$

where $\Omega_{\mu\nu} = \partial_\mu V_\nu - \partial_\nu V_\mu$ and $\mathbf{B}_{\mu\nu} = \partial_\mu\mathbf{b}_\nu - \partial_\nu\mathbf{b}_\mu - \Gamma_\rho(\mathbf{b}_\mu\times\mathbf{b}_\nu)$. The parameters of the models are as follows: the nucleon mass $M = 939$ MeV, the coupling parameters Γ_s,Γ_v,Γ_ρ of the mesons to the nucleons, the electron mass m_e, and the electromagnetic coupling constant $e = \sqrt{4\pi/137}$. In the above Lagrangian density $\boldsymbol{\tau}$ is the isospin operator. When density- dependent models are used, the nonlinear terms are not present and hence $\kappa = \lambda = \xi = 0$ and the density-dependent parameters are chosen as in [14,15,29]. When models with constant couplings are used, Γ_i is replaced by g_i, where $i = s, v, \rho$ as in [11,13]. The bulk nuclear matter properties of the models we use in the present paper are given in Table I. We also include in the table some properties at the thermodynamical spinodal surface: ρ_{spin} is the upper border density at the spinodal surface for symmetric matter (it defines

TABLE I. Nuclear matter properties at the saturation density and at the spinodal surface.

	NL3 [11]	GM1 [13]	TW [14]
B/A (MeV)	16.3	16.3	16.3
ρ_0 (fm^{-3})	0.148	0.153	0.153
K (MeV)	272	300	240
$\mathcal{E}_{\rm sym}$ (MeV)	37.4	32.5	32.8
M^*/M	0.60	0.70	0.55
L (MeV)	118.3	93.8	55.3
$K_{\rm sym}$ (MeV)	100.5	17.9	−124.7
Q_0 (MeV)	203	−216	−540
K_τ (MeV)	−698	−478	−332
$\rho_{\rm spin}$ (fm^{-3})	0.096	0.100	0.096
ρ_t (fm^{-3})	0.0646	0.0743	0.0850
P_t (MeV/fm^3)	0.396	0.382	0.455

the density for which the incompressibility is zero), and ρ_t and P_t are, respectively, the density and the pressure at the crossing between the cold β-equilibrium equation of state and the spinodal surface. They give a rough estimate of the density and pressure at the crust-core transition [6,8]. For symmetric matter or large proton fractions we expect that GM1 will have the largest extension of the pasta phase because it has the largest value of $\rho_{\rm spin}$. For cold β-equilibrium matter, TW predicts the largest pasta extension, with the largest transition density ρ_t.

From the de Euler–Lagrange formalism we obtain coupled differential equations for the scalar, vector, isovector-scalar, and nucleon fields. In the static case there are no currents and the spatial vector components are zero. In [6] a complete description of the mean field and Thomas-Fermi approximations applied to different parametrizations of the NLWM is given and we do not repeat it here. The equations of motion for the fields are obtained and solved self-consistently and they can be read off [6,8]. The above mentioned equations of motion depend on the the equilibrium densities $\rho = \rho_p + \rho_n$, $\rho_3 = \rho_p - \rho_n$, and $\rho_s = \rho_{sp} + \rho_{sn}$, where the proton and neutron densities are given by

$$\rho_i = \frac{1}{\pi^2}\int p^2 dp (f_{i+} - f_{i-}),\ \ i = p, n, \tag{9}$$

and the corresponding scalar density by

$$\rho_{s_i} = \frac{1}{\pi^2}\int p^2 dp \frac{M^*}{\sqrt{p^2 + M^{*2}}}(f_{i+} + f_{i-}), \tag{10}$$

with the distribution functions given by

$$f_{i\pm} = \frac{1}{1 + \exp[(\epsilon^*(\mathbf{p}) \mp \nu_i)/T]}\ , \tag{11}$$

where $\epsilon^* = \sqrt{\mathbf{p}^2 + M^{*2}}$,

$$M^* = M - \Gamma_s \phi_0, \tag{12}$$

and the effective chemical potentials are

$$\nu_i = \mu_i - \Gamma_v V_0 - \frac{\Gamma_\rho}{2}\tau_{3i} b_0 - \Sigma_0^R. \tag{13}$$

$\tau_{3i} = \pm 1$ is the isospin projection for the protons and neutrons, respectively. The density- dependent models in the mean field approximation contain a rearrangement term Σ_{0i}^R [15] given by

$$\Sigma_0^R = \frac{\partial \Gamma_v}{\partial \rho}(\rho) V_0 + \frac{\partial \Gamma_\rho}{\partial \rho}\rho_3 \frac{b_0}{2} - \frac{\partial \Gamma_s}{\partial \rho}\rho_s \phi_0.$$

In the description of the equations of state of a system, the required quantities are the baryonic density, energy density, pressure, and free energy, explicitly written in [6,8]. We refer next to only some of the quantities.

The free energy density is defined as

$$\mathcal{F} = \mathcal{E} - T\mathcal{S}, \tag{14}$$

with the entropy density

$$\mathcal{S} = \frac{1}{T}(\mathcal{E} + P - \mu_p \rho_p - \mu_n \rho_n). \tag{15}$$

In the present work the α particles are included as bosons and their chemical potential is obtained from the proton and neutron chemical potentials as in [24,26]:

$$\mu_\alpha = 2(\mu_p + \mu_n). \tag{16}$$

The inclusion of the α particles also gives rise to a rearrangement term given by

$$\Sigma_{0\alpha}^R = 4\frac{\partial \Gamma_\alpha}{\partial \rho}\rho_\alpha V_0, \tag{17}$$

which is present in the effective chemical potential of the α particles:

$$\nu_\alpha = \mu_\alpha - \Gamma_\alpha V_0 - \Sigma_{0\alpha}^R. \tag{18}$$

The density of α particles is

$$\rho_\alpha = \frac{1}{2\pi^2}\int p^2 dp (f_{\alpha+} - f_{\alpha-}), \tag{19}$$

with the boson distribution function given by

$$f_{\alpha\pm} = \frac{1}{-1 + \exp[(\epsilon_\alpha \mp \nu_\alpha)/T]}, \tag{20}$$

where $\epsilon_\alpha = \sqrt{p^2 + M_\alpha^2}$. The α free energy density reads

$$\mathcal{F}_\alpha = \mathcal{E}_\alpha - T\mathcal{S}_\alpha, \tag{21}$$

where $\mathcal{E}_\alpha$ and $\mathcal{S}_\alpha$ stand respectively for the bosonic energy and entropy density.

It is worth emphasizing that a term proportional to $\Sigma_{0\alpha}^R \rho_\alpha$ is present in the pressure. When nonlinear Walecka-type models are used there is no rearrangement term and the α effective chemical potential is also given by Eq. (16). For the temperatures we consider in the present work, no α-particle condensation occurs, and, therefore, the above equations do not contain the condensate contribution.

As for the electrons, their density and distribution functions read

$$\rho_e = \frac{1}{\pi^2}\int p^2 dp (f_{e+} - f_{e-}), \tag{22}$$

with

$$f_{e\pm}(\mathbf{r}, \mathbf{p}, t) = \frac{1}{1 + \exp[(\epsilon_e \mp \mu_e)/T]}, \tag{23}$$

where μ_e is the electron chemical potential and $\epsilon_e = \sqrt{p^2 + m_e^2}$. We always consider neutral matter, and therefore the electron density is equal to the charge density of the positive charged particles (protons and α particles).

The free energy density of the electrons reads

$$\mathcal{F}_e = \mathcal{E}_e - T\mathcal{S}_e, \tag{24}$$

with

$$\mathcal{S}_e = \frac{1}{T}(\mathcal{E}_e + P_e - \mu_e\rho_e). \tag{25}$$

III. COEXISTING PHASES

Two possibilities are discussed next: nuclear matter with fixed proton fraction and stellar matter with β equilibrium and trapped neutrinos.

A. Nuclear pasta

As in [5,6], for a given total density ρ and proton fraction, now defined with the inclusion of the protons present inside the α particles, the pasta structures are built with different geometrical forms in a background nucleon gas. This is achieved by calculating from the Gibbs conditions the density and the proton fraction of the pasta and of the background gas, so that in the whole we have to solve simultaneously the following six equations:

$$P^{\rm I}\left(\nu_p^{\rm I}, \nu_n^{\rm I}, M^{*\rm I}\right) = P^{\rm II}\left(\nu_p^{\rm II}, \nu_n^{\rm II}, M^{*\rm II}\right), \tag{26}$$

$$\mu_i^{\rm I} = \mu_i^{\rm II}, \quad i = p, n, \tag{27}$$

$$m_s^2\phi_0^{\rm I} + \frac{\kappa}{2}\phi_0^{2\rm I} + \frac{\lambda}{6}\phi_0^{3\rm I} = g_s\rho_s^{\rm I}, \tag{28}$$

$$m_s^2\phi_0^{\rm II} + \frac{\kappa}{2}\phi_0^{2\rm II} + \frac{\lambda}{6}\phi_0^{3\rm II} = g_s\rho_s^{\rm II}, \tag{29}$$

$$f\left(\rho_p^{\rm I} + 2\rho_\alpha^{\rm I}\right) + (1-f)\left(\rho_p^{\rm II} + 2\rho_\alpha^{\rm II}\right) = Y_p\rho, \tag{30}$$

where I and II label each of the phases; f is the volume fraction of phase I:

$$f = \frac{\rho - \rho^{\rm II}}{\rho^{\rm I} - \rho^{\rm II}}, \tag{31}$$

where the total baryonic density is

$$\rho = \rho_p + \rho_n + 4\rho_\alpha, \tag{32}$$

and Y_p is the global proton fraction given by

$$Y_p = \frac{\rho_p + 2\rho_\alpha}{\rho}. \tag{33}$$

The density of electrons is uniform and taken as $\rho_e = Y_p\rho$. The total pressure is given by $P = P^{\rm I} + P_e + P_\alpha$. The total energy density of the system is given by

$$\mathcal{E} = f\mathcal{E}^{\rm I} + (1-f)\mathcal{E}^{\rm II} + \mathcal{E}_e + \mathcal{E}_{\rm surf} + \mathcal{E}_{\rm Coul}, \tag{34}$$

where, by minimizing the sum $\mathcal{E}_{\rm surf} + \mathcal{E}_{\rm Coul}$ with respect to the size of the droplet or bubble, rod or tube, or slab we get [5]

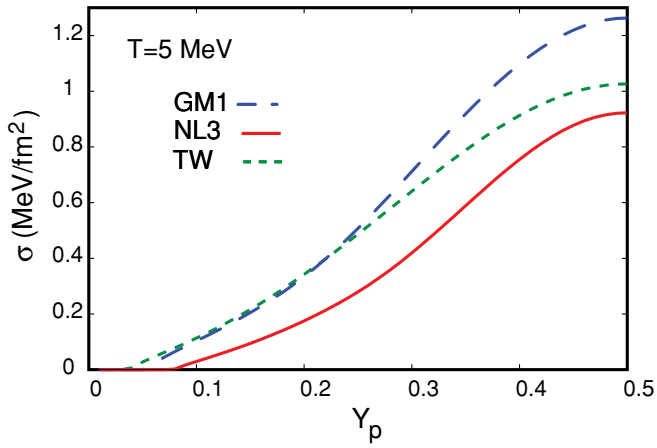

FIG. 1. (Color online) Surface energy as a function of the proton fraction for GM1, NL3, and TW parametrizations.

$\mathcal{E}_{\rm surf} = 2\mathcal{E}_{\rm Coul}$, and

$$\mathcal{E}_{\rm Coul} = \frac{2F}{4^{2/3}}(e^2\pi\Phi)^{1/3}\left[\sigma D\left(\rho_p^{\rm I} - \rho_p^{\rm II}\right)\right]^{2/3}, \tag{35}$$

where $F = f$ for droplets and $F = 1 - f$ for bubbles, σ is the surface energy coefficient, and D is the dimension of the system. For droplets, rods, and slabs,

$$\Phi = \begin{cases} \left(\frac{2-Df^{1-2/D}}{D-2} + f\right)\frac{1}{D+2}, & D = 1, 3, \\ \frac{f-1-\ln(f)}{D+2}, & D = 2, \end{cases} \tag{36}$$

and for bubbles and tubes the above expressions are valid with f replaced by $1 - f$.

Each structure is considered to be in the center of a charge-neutral Wigner-Seitz cell constituted by neutrons, protons and leptons [21]. The Wigner-Seitz cell is a sphere, cylinder, or slab whose volume is the same as the unit bcc cell. In [21] the internal structures are associated with heavy nuclei. Hence, the radius of the droplet (rod, slab) and of the Wigner-Seitz cell are respectively given by

$$R_D = \left(\frac{\sigma D}{4\pi e^2\left(\rho_p^I + 2\rho_\alpha^I - \rho_p^{II} - 2\rho_\alpha^{II}\right)^2\Phi}\right)^{1/3}, \tag{37}$$

$$R_W = \frac{R_D}{(1-f)^{1/D}}. \tag{38}$$

In Fig. 1 the surface energy is plotted as a function of the proton fraction for the three models under study. It is seen that the models differ a lot.

B. Surface energy

The authors of [30] have studied how the uncertainties on the surface energy affect the appearance of nonspherical pasta structures. In particular, they have shown that for typical values of the surface energy nonspherical clusters may occur below the transition density to uniform matter. Also the authors of [5] state that the appearance of the pasta phase essentially depends on the value of the surface tension. We have fixed the surface tension at different values and confirmed their claim in [6,8], where the surface energy coefficient was parametrized in terms

of the proton fraction according to the functional proposed in [31], obtained by fitting Thomas-Fermi and Hartree-Fock numerical values with a Skyrme force.

In the present paper we have considered this point in a more systematic and consistent way. Hence, we have parametrized the surface energy according to our Thomas-Fermi calculations for the relativistic models under investigation. We have used the Gibbs prescription to obtain the σ coefficient which, as extensively discussed in the literature [32,33], is the appropriate surface tension coefficient to be used. We have obtained for the three parametrizations used in this work, namely, NL3, TW, and GM1 parameter sets, the corresponding fittings for σ. Here, we briefly discuss the method that we have employed for fitting σ; more specific details about the numerical algorithm can be found in [6]. First, we obtain a density profile for the two-component system consisting of protons and neutrons in a semi-infinite one-dimensional system, where the axis perpendicular to the interface has been defined as the z axis. In our approach, we assume the system to be inside a large box of radius R so that the densities at the left and right boundaries correspond to asymptotic densities that approach the values of uniform nucleon matter (nucleus) in equilibrium with a gas of drip particles and a uniform gas of drip particles, respectively. Hence, we need a recipe in order to extract the surface energy from the bulk one. The surface tension may be expressed as follows:

$$\sigma = \int_{-\infty}^{\infty} dz\,[\epsilon(z) - \epsilon_d - \epsilon_{\rm ref}(z)] \tag{39}$$

as discussed in [32]. The quantity $\epsilon_{\rm ref}(z)$ corresponds to a reference energy density associated with the bulk contribution, $\epsilon_d = \lim_{z\to\infty}\epsilon(z)$, and $\epsilon(z)$ is the energy density. If one considers the Gibbs phase coexistence conditions and usual thermodynamic relations, one obtains for the (Gibbs) surface tension coefficient the expression

$$\sigma = \int_{-\infty}^{\infty} dz\{\epsilon(z) - \epsilon_d - \mu_n[\rho_n(z) - \rho_{nd}]. \\ - \mu_p[\rho_p(z) - \rho_{pd}]\},$$

with $\rho_{nd} = \lim_{z\to\infty}\rho_n(z)$ and an analogous definition for ρ_{pd}. An alternative and completely equivalent expression for the calculation of σ, known as the thin-wall approximation [34–36], is given by the following expression:

$$\sigma = \int_0^{\infty} dz\left[\left(\frac{d\phi_0}{dr}\right)^2 - \left(\frac{dV_0}{dr}\right)^2 - \left(\frac{db_0}{dr}\right)^2\right]. \tag{40}$$

In our parametrization of σ the above expression has been used since it is more convenient for our Thomas-Fermi numerical algorithm [6]. In particular, it is especially adequate for the parametrization of the dependence of σ on the temperature. We do not try to parametrize the σ through standard dimensionless functions which, as discussed in [33], do not give good fits for relativistic mean field models, especially for the region of small σ values which are important for the pasta study. So we follow a more pragmatic method, adopting a mathematical formula for σ that gives accurate results for a broad range of neutron excess and for temperatures up to 10 MeV, which are adequate for the studies addressed in the present work. The following functional for the surface tension coefficient σ is used:

$$\sigma = \sigma(x, T = 0)[1 - a(T)xT - b(T)T^2], \tag{41}$$

where $x = \delta^2$ stands for the squared relative neutron excess

$$\delta = \frac{\rho_n - \rho_p}{\rho} = 1 - 2Y_p,$$

and ρ, ρ_n, and ρ_p are defined at $z = -\infty$. A table with the coefficients $\sigma(x, T = 0)$, $a(T)$, and $b(T)$ for the NL3, TW, and GM1 parametrizations is shown in the Appendix. The proton fraction considered throughout the calculation of σ is the one of the denser phase.

C. Stellar pasta for matter in β equilibrium with trapped neutrinos

In this case, hadronic matter is in β equilibrium and the electron neutrinos are trapped. The condition of β equilibrium in a system of protons, neutrons, electrons, and neutrinos is

$$\mu_p = \mu_n - \mu_e + \mu_{\nu_e}. \tag{42}$$

In addition to the Gibbs conditions given in Eqs. (26), (27), (28), and (29) we also impose

$$Y_l = \frac{\rho_e + \rho_{\nu_e}}{\rho}, \tag{43}$$

where Y_l is the lepton fraction and has been fixed as 0.4 and ρ_{ν_e} is the density of electron neutrinos given by

$$\rho_{\nu_e} = \frac{1}{2\pi^2}\int p^2 dp\left(f_{\nu_{e+}} - f_{\nu_{e-}}\right), \tag{44}$$

with

$$f_{\nu_{e\pm}} = \frac{1}{1 + \exp\left[\left(p \mp \mu_{\nu_e}\right)/T\right]}. \tag{45}$$

The neutrino free energy density reads

$$\mathcal{F}_{\nu_e} = \mathcal{E}_{\nu_e} - T\mathcal{S}_{\nu_e}, \tag{46}$$

where $\mathcal{E}_{\nu_e}$ and $\mathcal{S}_{\nu_e}$ stand respectively for the neutrino energy and entropy density.

The densities of interest to the study of the pasta phase are too low for the muons to appear; they generally occur for densities above 0.1 fm^{-3} [18] and hence are not considered in the present work.

IV. RESULTS AND DISCUSSION

In this section we show results for the fraction of α particles in homogeneous matter and pastalike matter and discuss the effect of the α particles on the structure of the pasta phase.

A. α particles in homogeneous matter

We show the amount of α particles present in homogeneous nuclear matter described by the NL3 parametrization for symmetric matter and different temperatures in Fig. 2(a) and for $T = 5$ MeV and three proton fractions $Y_p = 0.5,\ 0.3,\ 0.1$ in Fig. 2(b). In all figures the curves drawn with thin lines were obtained for free α particles, $\Gamma_\alpha = 0$ and the curves

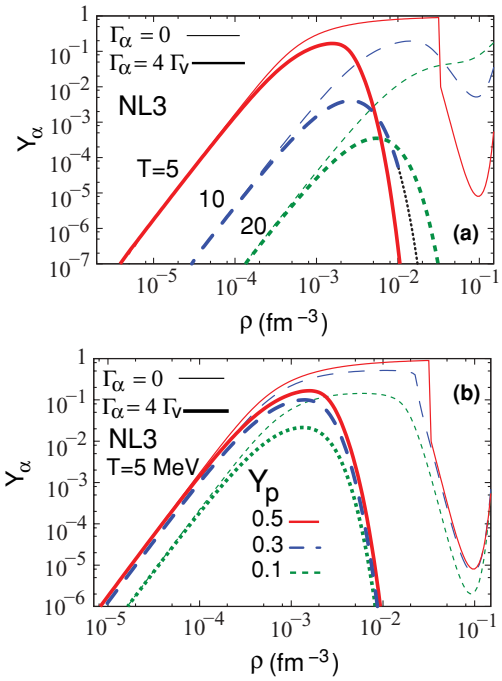

FIG. 2. (Color online) α fractions as a function of density for (a) symmetric matter and several temperatures and (b) $T = 5$ MeV and several proton fractions, obtained with NL3. The thin curves are for free α particles and the thick ones include the ω meson–α particle interaction.

with thick lines for $\Gamma_\alpha = 4\Gamma_v$, that is, with the inclusion of the term that mimics the excluded volume factor. As mentioned before, this term dissolves the clusters. In both calculations the α-particle vacuum mass was used. The maximum of the distribution occurs for the density that maximizes $2(\mu_p + \mu_n) - \Gamma_\alpha V_0 - M_\alpha$. The curves obtained with this term show the same behavior found in Fig. 15 of [24], that is, the α-particle fraction decreases with increase of the temperature. One can see from Fig. 2(b) that the total proton fraction Y_p has a different effect on the α-particle distribution. For $\Gamma_\alpha = 4\Gamma_v$, the maximum of the distribution occurs at the same density for all fractions, although the amount of α particles shows a lower value for the smaller value of Y_p. Moreover, the density of dissolution of α particles does not seem to be sensitive to the proton fraction, because it is defined by the isoscalar-vector interaction. The α-particle fractions for free α particles in Figs. 2(a) and 2(b) show discontinuities for large proton fractions at $T = 5$ MeV, just above $\rho = 0.02$ fm^{-3}. For lower proton fractions no discontinuity occurs. The region where the discontinuity occurs is a region of instability since the free energy has a negative concavity. For $T = 5$ MeV and $y_p = 0.3$ there is a smooth transition from a region with a large α-particle fraction to a region with a low α-particle fraction. If we increase the proton fraction the transition is no longer smooth and we obtain a jump in the α-particle fraction. The discontinuity occurs when the α-particle fraction becomes close to 1 and the chemical potential of the α particle is close to its mass. For larger densities the nucleon chemical potential decreases because of the attraction induced by the σ meson. The minimum of the nucleon chemical potential at

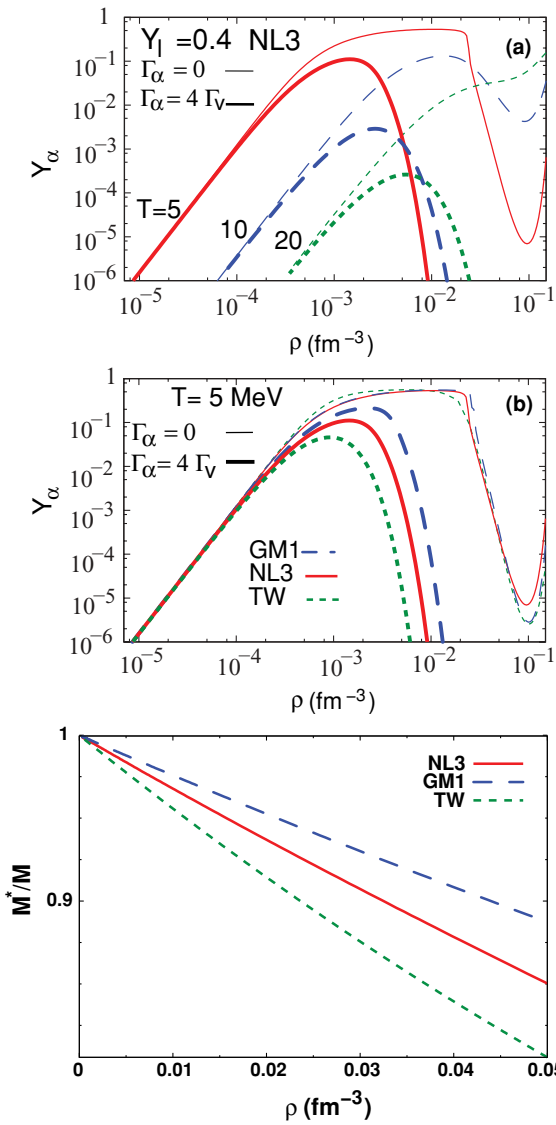

FIG. 3. (Color online) α fractions as a function of density obtained with (a) model NL3 for different temperatures; (b) models NL3, GM1, and TW for $T = 5$ MeV for matter in β equilibrium with trapped neutrinos. The thin curves are for free α particles and the thick ones include the ω meson–α particle interaction. In (c) the nucleon effective mass within NL3, GM1, and TW is plotted at subsaturation densities.

$\rho \sim 0.1$ fm^{-3} corresponds to the minimum of the α-particle fraction. The discontinuity or kink occurs at the density, or slightly above it, for which the nucleon chemical potential in the presence of α particles becomes equal to the nucleon chemical potential without α particles. To correctly treat this region of densities, where the free energy has a negative concavity, we should consider that matter is not homogeneous and there are two phases. However, to describe α particles as free particles is not realistic, and when the interaction between particles is included the discontinuity in the α-particle fraction does not occur.

In Fig. 3(a) the amount of α particles present in matter with β equilibrium and trapped neutrinos with the NL3

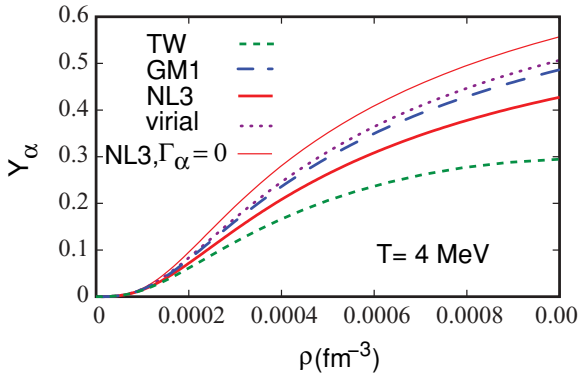

FIG. 4. (Color online) α fractions as a function of density obtained with GM1, NL3, and TW models compared with the virial EOS results of Ref. [23].

parametrization is displayed for different temperatures. Just as in Fig. 2(a), it is seen that the larger the temperature the lower the maximum of the α-particle distribution. With the increase of temperature, the maximum is shifted to larger densities and the same occurs to the dissolution of the clusters. This behavior was also obtained in [24]. However, in [24] other smaller clusters, besides the α particles, have also been considered. In Fig. 3(b) the same is shown for $T = 5$ MeV and the three models used in the present work. TW is responsible for the smallest amount of α particles and GM1 for the largest. These behaviors are defined by the model properties at subsaturation densities. This can be seen in Fig. 3(c), where the nucleon effective masses of NL3, GM1, and TW are plotted for subsaturation densities. If the nucleon mass is larger it becomes energetically more favorable to produce more α particles and fewer free nucleons. Both the cluster dissolution and the particle maximum occur at smaller densities for TW and larger densities for GM1 for the same reason. To a smaller effective mass corresponds a larger ω-meson coupling since the parameters of the models are chosen to reproduce the nuclear saturation properties.

The virial expansion gives a model-independent prediction of the low-density limit of the EOS [23]. In Fig. 4 we compare the α-particle fraction obtained with the virial EOS of low-density nuclear matter [23] with the prediction of the models GM1, NL3, and TW with interacting α particles, $\Gamma_\alpha = 4\Gamma_v$. We also include the NL3 results for free α particles (thin red line). The GM1 parametrization with interacting α particles gives the closest results to the virial expansion and TW deviates the most.

B. α particles in the pasta phase

In the following, we analyze the effect of the pasta phase on the fraction of α particles. The α particles are present in the background gas that surrounds the pasta structures.

In Fig. 5 we have plotted the α-particle fraction Y_α for $T = 5$ and 8 MeV with the proton fraction $Y_p = 0.3$. Notice that $Y_\alpha = 4\rho_\alpha/\rho$ is the fraction of nucleons clustered in α particles. In both figures we include the homogeneous matter results (dashed lines) and the pastalike matter results (full

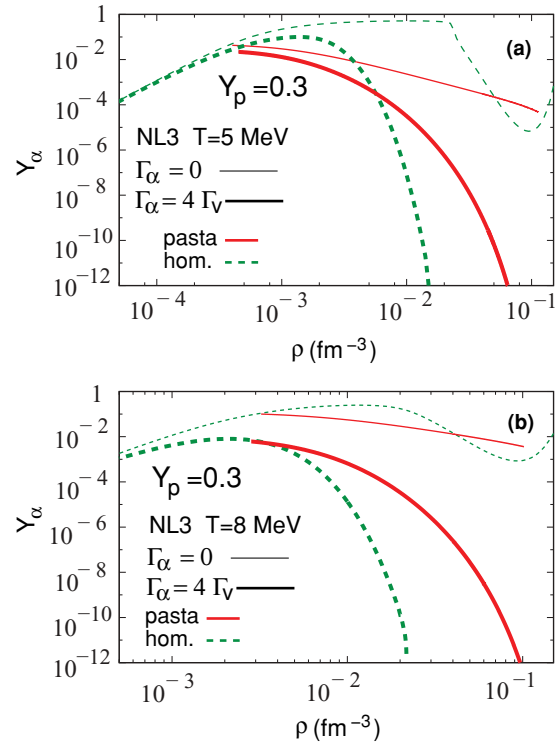

FIG. 5. (Color online) α fractions as a function of density obtained with model NL3 for (a) $Y_p = 0.3$ and $T = 5$ MeV; (b) $Y_p = 0.3$ and $T = 8$ MeV. The thin curves are for free α particles and the thick ones include the ω meson–α particle interaction.

lines). We have considered both free α particles (thin lines) and interacting α particles (thick lines). If free α particles are considered, the fraction Y_α in homogeneous matter becomes quite high and it may be close to 1, which is quite unrealistic. In pastalike matter the maximum of Y_α is smaller, but still quite high: it varies between ~0.01 and 0.1 and, for $Y_p = 0.3$, it is larger for larger temperatures, $T = 8$ MeV. This last tendency is still true when we include the interaction of α particles with the ω meson. If we analyze the results including the α-ω interaction some important conclusions can be drawn: while for homogeneous matter $Y_\alpha < 10^{-12}$ for $\rho > 0.02$ fm^{-3}, for pastalike matter this only occurs at the crust-core boundary for $\rho \sim 0.1$ fm^{-3}.

We may consider the prediction of Fig. 5 a lower bound prediction, since for the α-particle interaction we have considered only a repulsive interaction which mimics the volume exclusion effect. If attraction had also been considered we would expect larger fractions [24]. Also we have taken for the coupling constant the nucleon-meson coupling constant multiplied by the mass number, and this could be too strong a coupling. In pastalike matter for symmetric matter the α-particle fraction does not change because of the method used to calculate the pasta phase. Phase equilibrium for symmetric nuclear matter predicts the same proton fraction, equal to 0.5, as well as the same pressure for both the dense (liquid) and gas phases of the pasta. We may expect that within a Thomas-Fermi calculation the α-particle fraction changes with density.

From Fig. 6 it is seen again that the α-particle fraction is model dependent: GM1 predicts generally larger fractions

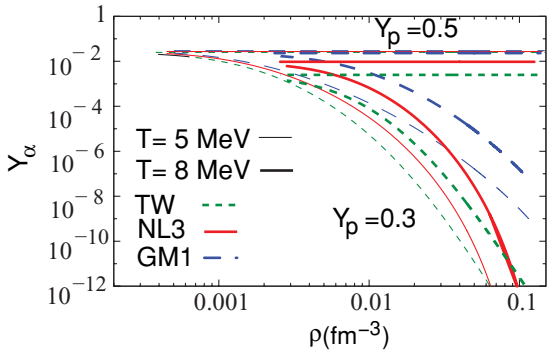

FIG. 6. (Color online) α fractions as a function of density obtained with the models under investigation for $Y_p = 0.5$ and 0.3 and $T = 5$ and 8 MeV. The thin curves are for $T = 5$ MeV and the thick curves for $T = 8$ MeV.

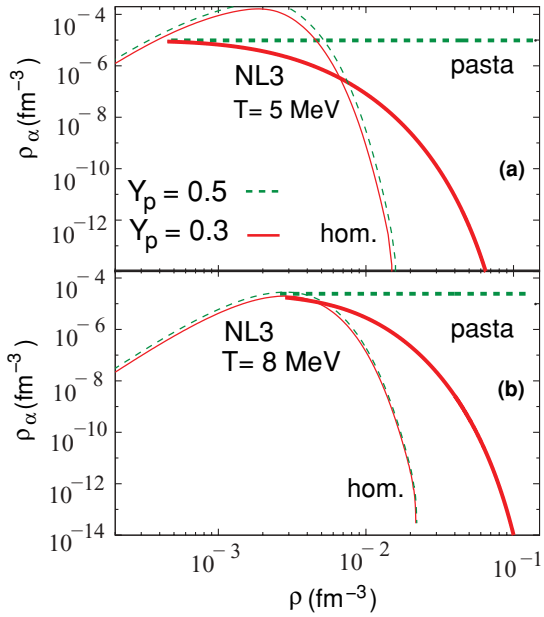

FIG. 7. (Color online) α-particle density for (a) $T = 5$ MeV and (b) $T = 8$ MeV and $Y_p = 0.3$ and 0.5 obtained with NL3 for homogeneous matter (thin lines) and gas phase of the pasta-like matter (thick lines). All calculations include the ω meson–α particle interaction.

although the difference depends on the density. The differences can be as high as one or two orders of magnitude. The magnitude of Y_α depends on the fraction of protons present in the background gas. The low-density onset of the pastalike matter in Figs. 5 and 6 lies slightly below the homogeneous matter curves. The difference is smaller for the larger temperatures owing to the distillation effect. The pasta phase starts at low density with small droplets of dense matter in a background gas. As soon as the droplets begin to form, the distillation effect makes matter in the droplet more proton-rich and that in the gas more proton-poor. Therefore, if we fix the global proton fraction, we expect that at the onset of the droplets (the volume fraction of the dense part is very small) the gas phase has a smaller proton fraction than the homogeneous matter at the corresponding density. This effect is smaller for larger temperatures and can be observed from Figs. 5 and 6.

The α-particle densities are plotted in Fig. 7 for two proton fractions ($Y_p = 0.5$ and 0.3) and two temperatures ($T = 5$ and 8 MeV). We include the calculation for both homogeneous and pastalike matter and we consider only the case of interacting α particles. This figure gives a hint as to the possible effects of α particles in the inner crust of a compact star. The effect is larger for the larger temperatures and larger proton fractions. Because of the existence of a nonhomogeneous phase, the presence of the α particles extends to larger densities. In fact the α clusters dissolve at $\rho \sim 0.01$ fm^{-3} in homogeneous matter. If we consider the pasta phase, the background gas does not exceed this value of the density and, therefore, there are still α clusters at much larger densities because they only exist in the gas phase. However, we should point out that, with the strongly repulsive interaction considered, Y_α takes very small values.

In Figs. 2(a) and 3(a) it is clearly seen that the maximum fraction of α particles decreases with temperature; however, clusters dissolve at larger densities and above 0.01 fm^{-3} the fraction of α particles is much larger for $T = 10$ MeV than for $T = 5$ MeV. This effect is still seen in the pasta phase, Fig. 7: above 0.01 fm^{-3} α-particle fractions are larger at $T = 8$ MeV than at $T = 5$ MeV.

It is worth emphasizing some points related to the effects of the α particles present in the inner crust of a compact star. They are small or negligible in calculations of the evolution of protoneutron stars because of the very low densities involved. However, simulations of supernova explosions seem to indicate that the internal structure of the pasta phase plays a decisive role in avoiding the stalling process. Moreover, at the inner crust the shear viscosity, thermal conductivity, and electrical conductivity are mainly determined by electron-ion scattering. Above neutron drip it is important also to consider electron-neutron scattering [37–39]. It has been shown [40] that the shear viscosity in the inner crust, which is mainly determined by electrons, is affected by the electron-impurity scattering at low temperatures. Recently, taking into account electron-proton scattering it was shown in [39] that the pasta structures would not increase the shear viscosity and thermal conductivity as expected, because of an effective reduction of the proton number of the clusters owing to ion screening effects. We expect that the presence of α particles will give an extra contribution that should be calculated. In this paper it was also shown that the scattering of neutrinos from neutrons would be defined by the difference between the neutron content of the pasta structures and the dripped neutron gas. The reduction of the background neutron gas due to the α-particle formation could increase the effective neutron content of the pasta structures.

In order to show the effect of the α-particle interaction on the background gas of the pasta phase, we plot in Fig. 8, for matter with trapped neutrinos and a lepton fraction $Y_l = 0.4$, the density ρ_α obtained with free and interacting particles. The α-particle density is lower for TW. A smaller α-particle fraction is due to the smaller symmetry energy for TW at

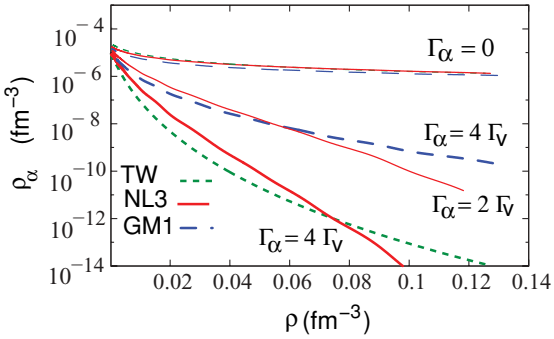

FIG. 8. (Color online) α-particle density in the gas phase of pastalike matter for $T = 5$ MeV and β-equilibrium matter with trapped neutrinos obtained with NL3, GM1, and TW. The α-particle density is given for three cases: free α particles $\Gamma_\alpha = 0$ (thin lines), interacting α particles with $\Gamma_\alpha = 4\Gamma_v$ (thick lines), and, just for NL3, interacting α particles with $\Gamma_\alpha = 2\Gamma_v$ (red medium thick line).

subsaturation densities, which does not favor the formation of isospin symmetric clusters. GM1, on the other hand, has the largest symmetry energy and predicts much larger α-particle fractions. We also conclude that it is crucial to know with accuracy the strength of the interaction to obtain the correct order of magnitude for Y_α. At $\rho = 0.08$ fm^{-3}, which corresponds approximately to the crust-core transition, the difference between a free α-particle gas and an interacting one with $\Gamma_\alpha = 4\Gamma_v$ could be as high as six orders of magnitude. Reducing the repulsive ω-α interaction to one half, $\Gamma_\alpha = 2\Gamma_v$, reduces the difference to three orders of magnitude. This test is shown only for NL3 and is represented in the figure by the red medium thick line, close to the GM1 result with $\Gamma_\alpha = 4\Gamma_v$.

C. Effect of the α particles on the phase transitions

In Fig. 9 we have plotted the free energy for homogeneous and pastalike matter described by the NL3 model with $T = 5$ MeV and proton fractions $Y_p = 0.5, 0.3$ and for β-equilibrium matter with trapped neutrinos for a lepton fraction $Y_l = 0.4$. The extension of the pasta free energy is determined by the binodal surface and becomes smaller when the proton fraction decreases. The system in equilibrium chooses the configuration with lower free energy so the pastalike matter defines the ground state of the system only while its free energy is lower than the free energy of the corresponding homogeneous matter.

In Tables II and III the densities at the crossing between the homogeneous and the pasta phases are given for NL3 and TW. The two crossing phases correspond to homogeneous matter to pasta (ρ_t^1 in the tables), at very low densities, and pasta to homogeneous matter (ρ_t^2 in the tables), at slightly higher densities. The corresponding pressures (P^1 and P^2 obtained in the pasta phase) are also given. The (*) means that the numbers shown for the crossing densities with NL3 and no α particles are different from the ones shown in [6] because a different parametrization for the surface energy was used here.

It is seen from Tables II and III that the transition density for symmetric matter is smaller than the transition density for

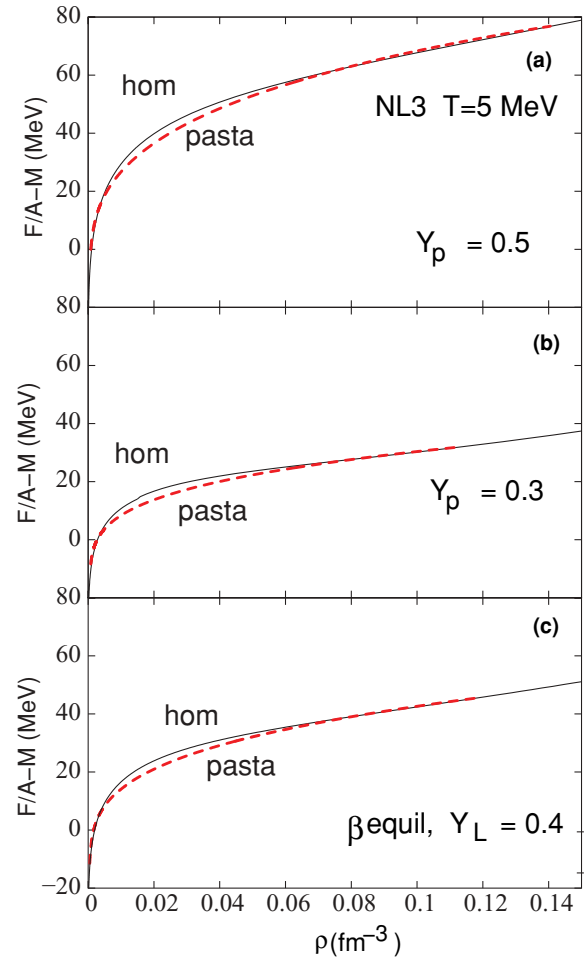

FIG. 9. (Color online) Free energy for the homogeneous and pastalike matter obtained within the NL3 for $T = 5$ MeV and several proton fractions. The red dashed line defines the pasta free energy and its extension is determined by the binodal. The crossings of the pasta and the homogeneous free energies define the extension of the pasta phase.

matter with $Y_p = 0.3$, while the opposite would be expected since the binodal has a smaller extension for the smaller proton fractions. In fact a Thomas- Fermi calculation predicts, respectively, 0.104 and 0.092 fm^{-3} for $Y_p = 0.5$ and $Y_p = 0.3$ for NL3 and $T = 5$ MeV [41]. As can be seen from Fig. 9, there is a range of densities close to the transition density when the free energies of pasta and homogeneous matter do not differ much. The same occurs with a Thomas-Fermi calculation. This corresponds to the range of densities that is sensitive to the method used and the self-consistency of the method. One large drawback of the coexisting phase method is the fact that the proton distribution inside the pasta structure is not perturbed by the Coulomb field. In particular, for symmetric matter the proton fraction of the structure is 0.5, larger than the prediction of a Thomas-Fermi calculation, which would predict that protons spread, giving rise to a smaller proton fraction, since the neutrons are not affected. This effect is larger the larger the proton fraction and is particularly critical for symmetric matter. We have verified that the density transition for symmetric matter at $T = 5$ MeV

TABLE II. Densities of the inner edge of the crust (crossing points) for NL3.

	EOS	ρ_t^1/ρ_t^2 (fm^{-3})	P^1/P^2 (MeV/fm^3)	Pasta structure
$T = 5$ MeV				
$Y_p = 0.5$				
	no α's (*)	0.004/0.077	0.039/2.065	Droplets, rods, slabs
	$\Gamma_{va} = 0$	0.010/0.077	0.155/2.069	Droplets, rods, slabs
	$\Gamma_{va} = 4\Gamma_v$	0.004/0.077	0.036/2.065	Droplets, rods, slabs
$Y_p = 0.3$				
	no α's (*)	0.003/0.082	0.015/1.136	Droplets, rods, slabs
	$\Gamma_{va} = 0$	0.006/0.082	0.044/1.138	Droplets, rods, slabs
	$\Gamma_{va} = 4\Gamma_v$	0.003/0.082	0.017/1.136	Droplets, rods, slabs
$Y_l = 0.4$				
	no α's	0.003/0.080	0.024/1.430	Droplets, rods, slabs
	$\Gamma_{va} = 0$	0.007/0.080	0.060/1.431	Droplets, rods, slabs
	$\Gamma_{va} = 4\Gamma_v$	0.003/0.080	0.024/1.430	Droplets, rods, slabs
$T = 8$ MeV				
$Y_p = 0.3$				
	no α's (*)	0.025/0.042	0.275/0.516	Droplets, rods
	$\Gamma_{va} = 0$	0.025/0.045	0.281/0.572	Droplets, rods
	$\Gamma_{va} = 4\Gamma_v$	0.025/0.042	0.275/0.515	Droplets, rods
$Y_l = 0.4$				
	no α's			
	$\Gamma_{va} = 0$	0.029/0.039	0.418/0.593	Droplets, rods
	$\Gamma_{va} = 4\Gamma_v$			

TABLE III. Densities of the inner edge of the crust (crossing points) for TW.

	EOS	ρ_t^1/ρ_t^2 (fm^{-3})	P^1/P^2 (MeV/fm^3)	Pasta structure
$T = 5$ MeV				
$Y_p = 0.5$				
	no α's (*)	0.004/0.079	0.037/2.060	Droplets, rods, slabs
	$\Gamma_{va} = 0$	0.012/0.079	0.160/2.067	Droplets, rods, slabs
	$\Gamma_{va} = 4\Gamma_v$	0.004/0.079	0.038/2.060	Droplets, rods, slabs
$Y_p = 0.3$				
	no α's (*)	0.003/0.086	0.018/1.209	Droplets, rods, slabs
	$\Gamma_{va} = 0$	0.007/0.086	0.049/1.211	Droplets, rods, slabs
	$\Gamma_{va} = 4\Gamma_v$	0.003/0.086	0.018/1.209	Droplets, rods, slabs
$Y_l = 0.4$				
	no α's (*)	0.004/0.085	0.028/1.536	Droplets, rods, slabs
	$\Gamma_{va} = 0$	0.008/0.085	0.072/1.534	Droplets, rods, slabs
	$\Gamma_{va} = 4\Gamma_v$	0.004/0.085	0.026/1.537	Droplets, rods, slabs
$T = 8$ MeV				
$Y_p = 0.5$				
	no α's (*)			
	$\Gamma_{va} = 0$	0.030/0.042	0.605/0.919	Droplets, rods
	$\Gamma_{va} = 4\Gamma_v$			
$Y_p = 0.3$				
	no α's (*)	0.021 0.054	0.221/0.714	Droplets, rods
	$\Gamma_{va} = 0$	0.024/0.056	0.263/0.747	Droplets, rods
	$\Gamma_{va} = 4\Gamma_v$	0.021/0.054	0.222/0.715	Droplets, rods
$Y_l = 0.4$				
	no α's (*)	0.023/0.050	0.306/0.816	Droplets, rods
	$\Gamma_{va} = 0$	0.026/0.050	0.389/0.818	Droplets, rods
	$\Gamma_{va} = 4\Gamma_v$	0.023/0.050	0.306/0.816	Droplets, rods

TABLE IV. Densities of the inner edge of the crust (crossing points) for $T = 5$ MeV and $\Gamma_\alpha = 4\Gamma_v$.

	ρ_t^1/ρ_t^2 (fm^{-3})			P^1/P^2 (MeV fm^{-3})		
	NL3	GM1	TW	NL3	GM1	TW
$Y_p = 0.5$	0.004/0.077	0.005/0.080	0.004/0.079	0.039/2.065	0.049/2.076	0.038/2.060
$Y_p = 0.3$	0.003/0.082	0.004/0.088	0.003/0.086	0.017/1.136	0.021/1.243	0.018/1.209
$Y_l = 0.4$	0.003/0.080	0.003/0.094	0.004/0.085	0.024/1.430	0.028/1.527	0.026/1.537

would increase to 0.087 fm^{-3} if the central proton fraction of the structure were reduced by 20% because of the Coulomb force.

The presence of the α particles has only a small effect on the pasta phase structure and on the size of the clusters. The largest effect occurs for the lower densities, namely, the low-density limit of the onset of the pasta phase, when a gas of free α particles is considered: this defines an upper limit of the possible effect. The density at the upper border may be slightly larger for temperatures and proton fractions close to the critical values above which the pasta phase disappears, like the results obtained for $T = 8$ MeV. The density at the lower border is generally larger due to the softer EOS for the homogeneous matter with α particles. Including the interaction of the α particles with the ω meson defines the extension of the pasta phase to the limits obtained without α particles. The effect of the model is mainly noticeable close to the critical values of temperature and proton fraction: in particular, for matter with trapped neutrinos at $T = 8$ MeV we predict a pasta phase within TW, with or without α particles; however, for NL3 there is a pasta phase only in the presence of noninteracting α particles. A more precise knowledge of the effect of α particles requires a self-consistent calculation, within, for instance a Thomas-Fermi calculation.

We have included in Tables II and III the pressure at the transition between the pasta phase and the homogeneous matter because it as been shown in [42] that this pressure defines the mass and moment of inertia of the crust of compact stars. The presence of α particles does not seem to have a large effect on the pressure at the transition.

At this point a comment on the effect of thermal fluctuations is in order. The problem of the effect of thermal fluctuations on the pasta structures has been studied in [43,44] and it was shown that thermally induced displacements of the rodlike and slablike nuclei could melt the lattice structure when these displacement are larger than the space available between the cluster and the boundary of the Wigner-Seitz cell. Using the elastic constants calculated in [43], the authors of [44] have calculated the critical temperatures above which the ordered configuration is destroyed. While for the rodlike clusters and for the densities and temperatures considered in our work the lattice would not be affected by the thermal fluctuations, for the slabs and densities considered $T = 5$ MeV is a limiting temperature.

Table IV allows a comparison between the models NL3, GM1, and TW at the crust-core transition for $T = 5$ MeV and several proton fractions. The values in this table include the effect of interacting α particles. GM1 predicts larger transition densities at the crust-core boundary. This reflects the larger binodal region this model presents.

V. CONCLUSIONS

In the present work we have studied the effect of α particles on warm low-density stellar matter as found in the inner edge of the crust of a protoneutron star. We have considered three different types of relativistic nuclear model: the parametrizations NL3 [11] and GM1 [13] of the nonlinear Walecka model with constant couplings and the TW parametrization of the density-dependent relativistic hadronic model [14] with density-dependent coupling parameters.

We first considered a homogeneous neutral gas formed by protons, neutrons, electrons, and α particles with a fixed proton fraction or in β equilibrium with trapped neutrinos. The α particles were described as a gas of bosons, and two opposite situations were considered: a free gas of α particles with binding energy 28.3 MeV was used with no interaction taken into account, and a gas of particles with binding energy 28.3 MeV interacting through the exchange of a ω meson which reduces the interaction to a repulsive interaction. It is expected that a realistic situation lies between these two extrema. The binding energy is density and temperature dependent, and in the approach made in [24] the inclusion of a term that describes the temperature and density dependence of the binding energy is essential to dissolve the clusters. In the present work this was not considered explicitly, because, in order to reduce the unknown α-particle couplings, the attractive σ meson–α interaction was not included. It was shown that the inclusion of the repulsive interaction is essential to avoid an overprediction of α particles above $\rho \sim 0.001$ fm^{-3}, and it is also the mechanism responsible for the dissolution of the α-particle clusters in the present approach. In the low-density limit ($\rho < 0.0001$ fm^{-3}) all models considered behave in a similar way: this behavior essentially coincides with the one predicted by the virial expansion [23] when the interparticle interaction is negligible, and the system behavior is model independent. The main differences between models occur for $\rho > 0.001$ fm^{-3} when the α-particle fraction differences between models may be as large as one order of magnitude or even larger. TW predicts the smallest fractions and GM1 the largest ones. Temperature shifts the maximum on the α-particle distribution and the density of cluster dissolution to larger densities, although the maximum values of the distributions themselves decrease with temperature. The maximum values of the α-particle distributions also decrease when the proton fraction decreases. However, the proton fraction has no effect

on the density localization of the maximum nor on the density of dissolution of the clusters.

We next investigated the pasta phase with α particles. We described the pasta phase using the method described in [5,6,8]: the coexisting phases are determined from Gibbs conditions and surface energy and Coulomb interaction are added *a posteriori*. For the surface energy we have used the parametrizations determined in terms of the proton fraction and the temperature using a Thomas-Fermi calculation. It was shown in [5,6,8] that the method of coexisting phases is very sensitive to the surface energy. We performed our calculations for two temperatures $T = 5$ and 8 MeV, two proton fractions $Y_p = 0.5$ and 0.3, and for β-equilibrium matter with trapped neutrinos and a lepton fraction of 0.4. We analyzed the fraction of α particles as a function of density in the pasta phase and, comparing with the fraction of α particles in homogeneous matter, it was shown that it was larger by many orders of magnitude for densities above 0.01 fm^{-3}. It is important to stress that the prediction obtained within a homogeneous EOS calculation underestimates the α-particle fraction. This certainly affects transport properties such as heat conduction and electrical conductivity.

It was also seen that, while for symmetric matter the α-particle fraction decreases with temperature when interacting α particles are considered, for $Y_p = 0.3$ the opposite occurs. This is an interesting effect related to the proton fraction in the background gas, which increases with temperature for asymmetric matter.

Finally we analyzed the effect of the α particles on the pasta structure. It was shown that the effect is small except close to the critical temperatures and/or proton fractions when it may still predict a pasta phase, while no pasta phase would occur in the absence of light clusters. A self-consistent calculation is necessary to give more quantitative predictions. Other small clusters should also be included in the calculation.

ACKNOWLEDGMENTS

This work was partially supported by Capes/FCT n. 232/09 bilateral collaboration, by CNPq (Brazil), by FCT and FEDER (Portugal) under the project CERN/FP/109316/2009, and by Compstar, an ESF Research Networking Program.

APPENDIX

The surface tension coefficient σ, was calculated in the Thomas-Fermi approximation and fitted to the functional form given in Eq. (41), with $\sigma(x) = \sigma(x, T = 0)$, $a(T)$, and $b(T)$ having the following expressions:

$$\sigma(x) = \sigma_0 \exp(-\sigma_1 x^{3/2})(1 + a_1 x + a_2 x^2 + a_3 x^3 + a_4 x^4 + a_5 x^5 + a_6 x^6),$$
$$a(T) = a_0 + a_1 T + a_2 T^2 + a_3 T^3,$$
$$b(T) = a_0 + a_1 T + a_2 T^2 + a_3 T^3.$$

The results of the model fitting using the Thomas-Fermi approximation for the GM1, NL3, and TW parametrizations are given in Table V for temperatures up to $T = 10$ MeV.

TABLE V. Surface tension coefficient parameters fitted within the Thomas-Fermi approximation for GM1 [13], NL3 [11], and TW [14] parametrizations.

GM1	$\sigma(x)$	$a(T)$	$b(T)$
σ_0	1.488 01		
σ_1	10.6647		
a_0		0.005 215 94	0.006 408 79
a_1	−4.324 19	0.012 518 7	0.000 140 886
a_2	61.6172	−0.001 569 99	$-4.176\,15\times10^{-5}$
a_3	−488.383	8.4792×10^{-5}	1.6856×10^{-6}
a_4	1678.95		
a_5	−2450.41		
a_6	1296.86		
NL3	$\sigma(x)$	$a(T)$	$b(T)$
σ_0	1.123 07		
σ_1	20.7779		
a_0		0.012 122 2	0.007 921 68
a_1	−5.849 15	0.016 64	-8.2504×10^{-5}
a_2	138.839	−0.001 372 66	$-4.593\,36\times10^{-6}$
a_3	−1631.42	4.0257×10^{-5}	$-2.816\,79\times10^{-7}$
a_4	8900.34		
a_5	−21 592.3		
a_6	20 858.6		
TW	$\sigma(x)$	$a(T)$	$b(T)$
σ_0	1.217 35		
σ_1	8.334 25		
a_0		−0.004 818 23	0.008 446 64
a_1	−2.180 75	0.006 649 8	$-7.233\,79\times10^{-4}$
a_2	18.0584	−0.000 267 288	9.6817×10^{-5}
a_3	−96.548	$1.345\,44\times10^{-5}$	$-5.084\,88\times10^{-6}$
a_4	259.517		
a_5	−296.69		
a_6	125.94		

[1] D. G. Ravenhall, C. J. Pethick, and J. R. Wilson, Phys. Rev. Lett. **50**, 2066 (1983).
[2] M. Hashimoto, H. Seki, and M. Yamada, Prog. Theor. Phys. **71**, 320 (1984).
[3] C. J. Horowitz, M. A. Pérez-Garcia, and J. Piekarewicz, Phys. Rev. C **69**, 045804 (2004); C. J. Horowitz, M. A. Pérez-Garcia, D. K. Berry, and J. Piekarewicz, *ibid.* **72**, 035801 (2005).
[4] G. Watanabe, K. Sato, K. Yasuoka, and T. Ebisuzaki, Phys. Rev. C **66**, 012801 (2002); **68**, 035806 (2003); **69**, 055805 (2004); H. Sonoda, G. Watanabe, K. Sato, K. Yasuoka, and T. Ebisuzaki, *ibid.* **77**, 035806 (2008).
[5] T. Maruyama, T. Tatsumi, D. N. Voskresensky, T. Tanigawa, and S. Chiba, Phys. Rev. C **72**, 015802 (2005).
[6] S. S. Avancini, D. P. Menezes, M. D. Alloy, J. R. Marinelli, M. M. W. Moraes, and C. Providência, Phys. Rev. C **78**, 015802 (2008).
[7] J. Xu, L. W. Chen, B. A. Li, and H. R. Ma, Phys. Rev. C **79**, 035802 (2009).

[8] S. S. Avancini, L. Brito, J. R. Marinelli, D. P. Menezes, M. M. W. de Moraes, C. Providência, and A. M. Santos, Phys. Rev. C **79**, 035804 (2009).
[9] G. Watanabe and H. Sonoda, arXiv:cond-mat/0502515v2 [cond-mat.soft].
[10] B. Serot and J. D. Walecka, Adv. Nucl. Phys. **16**, 1 (1986).
[11] G. A. Lalazissis, J. König, and P. Ring, Phys. Rev. C **55**, 540 (1997).
[12] K. Sumiyoshi, H. Kuwabara, and H. Toki, Nucl. Phys. A **581**, 725 (1995).
[13] N. K. Glendenning, *Compact Stars* (Springer-Verlag, New York, 2000).
[14] S. Typel and H. H. Wolter, Nucl. Phys. A **656**, 331 (1999); Guo Hua, Liu Bo, and M. Di Toro, Phys. Rev. C **62**, 035203 (2000).
[15] T. Gaitanos, M. Di Toro, S. Typel, V. Baran, C. Fuchs, V. Greco, and H. H. Wolter, Nucl. Phys. A **732**, 24 (2004).
[16] P. Gögelein, E. N. E. van Dalen, C. Fuchs, and H. Müther, Phys. Rev. C **77**, 025802 (2008).
[17] E. N. E. van Dalen, C. Fuchs, and A. Faessler, Eur. Phys. J. A **31**, 29 (2007).
[18] C. Ducoin, C. Providência, A. M. Santos, L. Brito, and Ph. Chomaz, Phys. Rev. C **78**, 055801 (2008).
[19] G. Watanabe, H. Sonoda, T. Maruyama, K. Sato, K. Yasuoka, and T. Ebisuzaki, Phys. Rev. Lett. **103**, 121101 (2009).
[20] J. M. Lattimer and F. D. Swesty, Nucl. Phys. A **535**, 331 (1991).
[21] H. Shen, H. Toki, K. Oyamatsu, and K. Sumiyoshi, Nucl. Phys. A **637**, 435 (1998).
[22] M. Beyer, S. A. Sofianos, C. Kuhrts, G. Röpke, and P. Schuck, Phys. Lett. B **488**, 247 (2000).
[23] C. J. Horowitz and A. Schwenk, Nucl. Phys. A **776**, 55 (2006).
[24] S. Typel, G. Röpke, T. Klähn, D. Blaschke, and H. H. Wolter, Phys. Rev. C **81**, 015803 (2010).
[25] H. Shen, H. Toki, K. Oyamatsu, and K. Sumiyoshi (private communication).
[26] W. R. Hix, F. K. Thielemann, I. Fushiki, and J. W. Truran (private communication).
[27] G. Roepke, A. Grigo, K. Sumiyoshi, and H. Shen, NATO Science Series, Series II: Mathematics, Physics and Chemistry **197**, 75 (2006).
[28] S. S. Avancini, L. Brito, Ph. Chomaz, D. P. Menezes, and C. Providência, Phys. Rev. C **74**, 024317 (2006); H. Pais, A. Santos, and C. Providência, *ibid.* **80**, 045808 (2009).
[29] S. S. Avancini, L. Brito, D. P. Menezes, and C. Providência, Phys. Rev. C **70**, 015203 (2004).
[30] G. Watanabe, K. Iida, and K. Sato, Nucl. Phys. A **676**, 455 (2000); **687**, 512 (2001); **726**, 357 (2003).
[31] J. M. Lattimer, C. J. Pethick, D. G. Ravenhall, and D. Q. Lamb, Nucl. Phys. A **432**, 646 (1985).
[32] M. Centelles, M. Del Estal, and X. Viñas, Nucl. Phys. A **635**, 193 (1998).
[33] W. D. Myers and W. J. Swiatecki, Phys. Rev. C **63**, 034318 (2001).
[34] M. Nielsen and J. da Providência, J. Phys. G **16**, 649 (1990).
[35] C. da Providência, L. Brito, J. da Providência, M. Nielsen, and X. Viñas, Phys. Rev. C **54**, 2525 (1996).
[36] D. P. Menezes and C. Providência, Phys. Rev. C **60**, 024313 (1999).
[37] E. Flowers and N. Itoh, Astrophys. J. **206**, 218 (1976).
[38] A. I. Chugonov and D. G. Yakovlev, Astron. Rep. **49**, 814 (2005).
[39] C. J. Horowitz and D. K. Berry, Phys. Rev. C **78**, 035806 (2008).
[40] Nicolas Chamel and Pawel Haensel, Living Rev. Relativ. **11**, 10 (2008) [http://www.livingreviews.org/lrr-2008-10].
[41] S. S. Avancini, J. R. Marinelli, D. P. Menezes, M. M. W. Moraes, C. Providência, A. M. Santos, Int. J. Mod. Phys. D (to be published).
[42] C. J. Pethick and D. G. Ravenhall, Annu. Rev. Nucl. Part. Sci. **45**, 429 (1995).
[43] C. J. Pethick and A. Y. Potekhin, Phys. Lett. B **427**, 7 (1998).
[44] G. Watanabe, K. Iida, and K. Sato, Nucl. Phys. A **676**, 455 (2000); **726**, 357 (2003).